Theoretical Studies of Biological Nitrogen Fixation. I. Density Functional Modeling of the Mo-Site of the FeMo-Cofactor

Robert K. Szilagyi, Djamaladdin G. Musaev,* and Keiji Morokuma*

Cherry L. Emerson Center for Scientific Computation and Department of Chemistry, Emory University, Atlanta, Georgia 30322

Received February 22, 2000

The Mo-site and its ligand environment of the FeMo-cofactor (FeMo-co) were studied using the hybrid density functional method B3LYP. The structure and stability of the model complex (S-ligand)$_3$(N-ligand)Mo[*(S)*-OCH(CH$_3$)C(O)O−] along with its various protonated and reduced/oxidized forms were calculated. Several hypotheses were tested: (i) ligand environment of the Mo-site, (ii) monodentate vs bidentate coordination of the Mo-bound homocitrate ligand, (iii) substrate coordination to the Mo center, and (iv) Mo-*His* interaction. It was found that the decoordination of one of the homocitrate (lactate in the model) "legs", the bidentate → monodentate rearrangement, does not occur spontaneously upon either single/double protonation or one-electron reduction. However, it could occur only upon substrate coordination to the Mo-center of the single-protonated forms of the complex. It was shown that one-electron reduction, single-protonation, and substrate coordination facilitate the bidentate ↔ monodentate rearrangement of the homocitrate (lactate) ligand of FeMo-co. It was demonstrated that the smallest acceptable model of *His* ligand in FeMo-co is methylimidazolate (MeIm$^-$). Our studies suggest that the ϵ-N of the FeMo-co-bound *His* residue is not protonated, and as a consequence the cluster is tightly bound to the protein matrix via a strong Mo−N$^\delta$ bond.

I. Introduction

Nitrogenase is an enzyme that converts dinitrogen to ammonia by a sequence of electron- and proton-transfer reactions (eq 1).[1−2]

$$N_2 + 8e^- + 8H^+ + 16MgATP \rightarrow 2NH_3 + H_2 + 16MgADP + 16P(phosphate) \quad (1)$$

In the literature,[3] three different nitrogenases (so-called Mo-, V- and Fe-nitrogenase) have been reported. While their catalytic behavior is quite similar, some differences should be mentioned.[4] First, the V- and Fe-nitrogenases can reduce acetylene to ethane, while the Mo-nitrogenase reduces it only to ethylene. Second, ammonia is the only product in nitrogen fixation by Mo-nitrogenase, while the formation of hydrazine was also observed for the V- and Fe-nitrogenases. Third, the ratio of proton and nitrogen reduction abilities of Mo-:V-:Fe-nitrogenases is 8:5:1 and 3:2:1, respectively. As the most active and the most studied one among the three nitrogenases, below we discuss only the Mo-nitrogenase in more detail.

X-ray diffraction studies[5−10] show that the Mo-nitrogenase contains two proteins, FeMo- and Fe-proteins. The FeMo-protein is an $\alpha_2\beta_2$ tetramer and contains several Fe and Mo atoms, which are distributed between two types of clusters, the "P"-cluster ([8Fe-7S]) and the FeMo-co ([7Fe-Mo-9S], known also as the "M"-center). Each $\alpha\beta$-pair of the FeMo-protein contains one "P"-cluster and one FeMo-co, which function independently. The second component of nitrogenase, Fe-protein, contains two identical subunits bridged by a single [4Fe-4S] cluster ("F"-center).[11] It is believed[12] that during the catalytic turnover, the Fe-protein acts as an electron source, and the "P"-cluster mediates electron-transfer from the "F"-cluster to the FeMo-co, where dinitrogen coordination and reduction occurs.

As shown in Scheme 1, the FeMo-co originating from *Azotobacter vinelandii (Av)*[13] contains one tetrahedral and six trigonal Fe atoms, an octahedral Mo atom, six tricoordinate (between tetrahedral Fe and trigonal Fe atoms, and octahedral Mo and trigonal Fe atoms) and three bicoordinate S atoms (between the central, trigonal Fe atoms), and a homocitrate ((2*R*)-hydroxybutane-1,2,4-tricarboxylic acid) ligand. It is bound to the polypeptide backbone through a cysteine sulfur (αCys275) to the unique tetrahedral Fe atom and a histidine residue (α*His*442) to the Mo atom. Spectroscopic studies (such as EPR, ENDOR, and Mössbauer[14−21]) of the FeMo-co in *Av* have shown that (1) the ground state of the resting form of FeMo-co has an $S = 3/2$ spin, (2) the Mo atom is an even-electron ion,

(1) Howard, J. B.; Rees, D. C. *Chem. Rev.* **1996**, *96*, 2965.
(2) Burgess, B. K.; Lowe, D. J. *Chem. Rev.* **1996**, *96*, 2983.
(3) Eady, R. R. *Chem. Rev.* **1996**, *96*, 3013.
(4) Eady, R. R. *Adv. Inorg. Chem.* **1991**, *36*, 77.
(5) Kim, J.; Rees, D. C. *Nature* **1992**, *360*, 553.
(6) Kim, J.; Rees, D. C. *Science* **1992**, *257*, 1677.
(7) Dees, D. C.; Chan, M. K.; Kim, J. *Adv. Inorg. Chem.* **1993**, *40*, 89.
(8) Bolin, J. T.; Ronco, A. E.; Morgan, T. V.; Mortenson, L. E.; Xuong, N. H. *Proc. Natl. Acad. Sci. U.S.A.* **1993**, *90*, 1078.
(9) Chan, M. K.; Kim, J.; Rees, D. C. *Science* **1993**, *260*, 792.
(10) Peters, J. W.; Stowell, M. H. B.; Soltis, S. M.; Finnegan, M. G.; Johnson, M. K.; Rees, D. C. *Biochem.* **1997**, *36*, 1181.
(11) Georgiadis, M. M.; Komiya, H.; Chakrabarti, P.; Woo, D.; Kornuc, J. J.; Rees, D. C. *Science* **1992**, *257*, 1653.
(12) Thorneley, R. N. F.; Ashby, G. A.; Fisher, K.; Lowe, D. J. *ASC Symp. Ser.* **1993**, *535*, 290.
(13) Thorneley, R. *J. Biol. Inorg. Chem.* **1996**, *1*, 575.
(14) Burgess, B. K. *Chem. Rev.* **1990**, *90*, 1377.
(15) Newton, W. E. In *Biological Nitrogen Fixation*; Stacey, G., Burris, R. H., Evans, H. J., Eds.; Chapman and Hall, New York, 1992; 877.
(16) Yang, S.,-S.; Pan, W.,-H.; Friessen, G. D.; Burgess, B. K.; Corbin, J. L.; Stiefel, E. I.; Newton, W. E. *J. Biol. Chem.* **1982**, *257*, 8042.
(17) Eady, R. R.; Imam, S.; Lowe, D. J.; Miller, R. W.; Smith, B. E.; Thorneley, R. N. F. In *Nitrogen Fixation*; Stewart, W. D. P., Gallon, J. R., Eds.; Academic Press: New York, 1980; 19.

10.1021/ic000188n CCC: $20.00
Published on Web 01/12/2001

Scheme 1

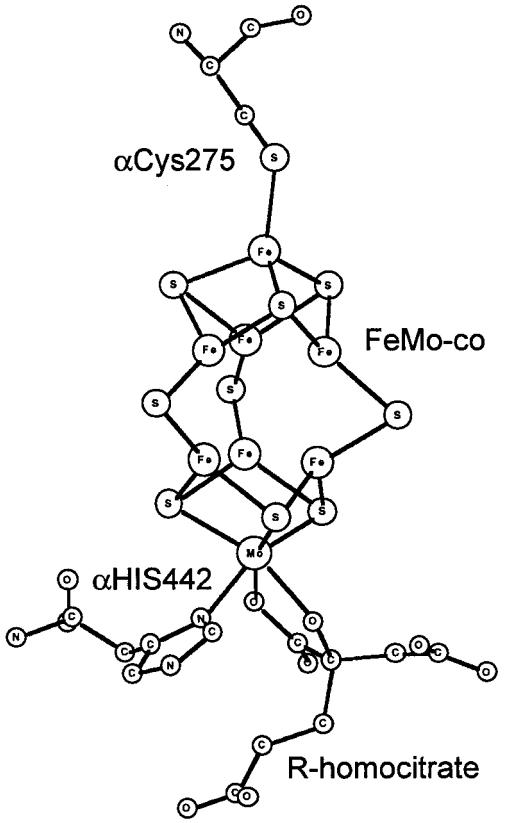

most probably Mo^{IV}, and (3) there are five distinct Fe sites: three A (mixed valence pairs Fe^{II}/Fe^{III})-type and two B (Fe^{II} ferrous ions)-type sites.[22−25]

In the literature, several mechanisms for nitrogenase have been proposed, among which a widely accepted one is the Thorneley−Lowe mechanism.[26] This mechanism assumes that eight Fe-protein cycles are required for transferring eight electrons and eight protons to reduce dinitrogen to ammonia and to evolve dihydrogen on the FeMo-co. However, neither the way this cluster binds and activates dinitrogen nor the role of its protein and ligand environment is well understood.

First, experimental studies show that the FeMo-co alone cannot perform the dinitrogen reduction chemistry, and its protein environment is important. Indeed, it was shown, that the extracted [7Fe-Mo-9S] cluster[27] is inactive in N_2 reduction,[14,15] while it can reduce substrates[28−30] such as N_2H_2 and CN^-. Crucial evidence that the FeMo-co is a place where the N_2 fixation takes place is that the apo-enzyme (lack of the FeMo-co) itself does not show the N_2 reduction activity nor the characteristic $S = 3/2$ EPR signal.[20,31] However, addition of isolated FeMo-co to these apo-enzyme strains results in recovery of activity and EPR signals.

Second, mutation studies[32] show the importance of the ligand environment of the FeMo-co. It was found that the mutant nitrogenases containing citrate ligand[33] instead of homocitrate has a very low nitrogen and hydrogen reduction abilities.[34,35] This difference in reactivity led to the assumption that the homocitrate ligand is anchoring the [7Fe-Mo-9S] cluster in the protein cavity and tunes its relative position to the protein surrounding.[36] In the case of the citrate, where both "carboxylic arms" are identical, this steric adjustment cannot be achieved. However, the homocitrate ligand may have other roles in the catalytic activity of the nitrogenase.[37,38] Studies on the reactivity of cluster $[(L)(L')Fe_3MoS_4Cl_4]^{2+}$ (L is solvent CH_3CN, methylamine, or imidazole, and L′ is tetrachlorobenzene-1,2-diolato or polycarboxylato ligands) with hydrazine[39] and *cis*-dimethyldiazene[40] indicate that the coordinatively saturated Mo atom complexing the hydroxyl/carboxyl ligand can be activated and involved in the reduction process.

The third issue is the nature of active site, where dinitrogen coordination and reduction occurs. The CO-inhibition experiments[41] and biomimicking reactions[42] suggest the multiple active sites in the nitrogen fixation process. Most probably, they are coordinatively unsaturated six trigonal Fe atoms of the central prism of the cluster (see Scheme 1) and a possible pentacoordinate Mo-site after the protonation one of the coordinated oxygen atoms of the homocitrate ligand followed by its dissociation.

Several theoretical studies[43−54] were already published to provide more insights into this fascinating chemistry. All of these

(18) Smith, B. E.; Bishop, P. E.; Dixon, R. A.; Eady, R. R.; Filler, W. A.; Lowe, D. J.; Richards, A. J. M.; Thomson, A. J.; Thorneley, R. N. F.; Postgate, J. R. In *Nitrogen Fixation Research Progress*; Evans, H. J., Bottomley, P. J., Newton, W. E., Eds.; Martinus Nijhoff: Dordrecht, 1985; 597.
(19) Rawlings, J.; Shah, V. K.; Chisnell, J. R.; Brill, W. J.; Zimmerman, R.; Munck, E.; Orme-Johnson, W H. *J. Biol. Chem.* **1978**, *253*, 1001.
(20) Shah, V. K.; Davis, L. C.; Gordon, J. K.; Orme-Johnson, W. H.; Brill, W. J. *Biochim. Biophys. Acta* **1973**, *292*, 246.
(21) Christou, G.; Mascharak, P. K.; Armstrong, W. H.; Papaefthymiou, G. C.; Frankel, R. B.; Holm, R. H. *J. Am. Chem. Soc.* **1982**, *104*, 4711.
(22) Venters, R. A.; Nelson, M. J.; McLean, P. A.; True, A. E.; Levy, M. A.; Hoffman, B. M.; Orme-Johnson, W. H. *J. Am. Chem. Soc.* **1986**, *108*, 3487.
(23) Hoffman, B. M.; Roberts, J. E.; Orme-Johnson, W. H. *J. Am. Chem. Soc.* **1982**, *104*, 860.
(24) Venters, R. A.; Nelson, M. J.; McLean, P. A. *J. Am. Chem. Soc.* **1986**, *108*, 8, 3487.
(25) Hoffman, B. M.; Venters, R. A.; Roberts, J. E.; Nelson, M. J.; Orme-Johnson, W. H. *J. Am. Chem. Soc.* **1982**, *104*, 4711.
(26) Thorneley, R. N. F.; Lowe, D. J. In *Molybdenum Enzymes*; Spiro, T. G., Ed.; Wiley-Interscience: New York, 1985; 221.
(27) Shah, V. K.,; Brill, W. J. *Proc. Natl. Acad. Sci. U.S.A.* **1977**, *74*, 3249.
(28) Shah, V. K.; Chisnell, J. R.; Brill, W. J. *Biochem. Biophys. Res. Commun.* **1978**, *81*, 232.
(29) McKenna, C. E.; Jones, J. B.; Eran, H.; Huang, C. W. *Nature* **1979**, *280*, 611.
(30) Grönberg, K. L.; Gormal, C. A.; Smith, B. E.; Henderson, R. A. *Chem. Commun*. **1997**, 713.
(31) Madden, M. S.; Kindon, N. D.; Ludden, P. W.; Shah, V. K. *Proc. Natl. Acad. Sci. U.S.A.* **1990**, *87*, 6517.
(32) Bolin, J. T.; Campobasso, N.; Muchmore, S. W.; Morgan, T. V.; Mortenson, L. E. *ACS Symp. Ser.* **1993**, *535*, 186.
(33) Liang, J.; Madden, M.; Shah, V. K.; Burris, R. H. *Biochemistry* **1990**, *29*, 8577.
(34) McLean, P. A.; Dixon, R. A. *Nature* **1981**, *292*, 655.
(35) Hawkes, T. R.; McLean, P. A.; Smith, B. E. *J. Biochem*. **1984**, *217*, 317.
(36) Ludden, P. W.; Shah, V. K.; Roberts, G. P.; Homer, M.; Allen, R.; Paustian, T.; Roll, J.; Chatterjee, R.; Madden, M.; Allen, J. *ACS Symp. Ser*. **1993**, *535*, 196.
(37) Coucovanis, D.; Demandis, K. D.; Malinak, S. M.; Mosier, P. E.; Tyson, M. A.; Laughlin, L. J. *ACS Symp. Ser.* **1996**, *653*, 117.
(38) Pickett, C. J. *J. Biol. Inorg. Chem.* **1996**, *1*, 601.
(39) Demandis, K. D.; Malinak, S. M.; Coucouvanis, D. *Inorg. Chem.* **1996**, *35*, 4038.
(40) Malinak, S. M.; Simeonov, A. M.; Moiser, P. E.; McKenna, C. E.; Coucouvanis, D. *J. Am. Chem. Soc.* **1997**, *119*, 1662.
(41) Burgess, B. K. *ACS Symp. Ser.* **1993**, *535*, 143.
(42) Coucovanis, D. *Acc. Chem. Res.* **1991**, *24*, 1.
(43) Deng, H.; Hoffmann, R. *Angew. Chem., Int. Ed. Engl*. **1993**, *32*, 1062.
(44) Dance, I. G. *Australian. J. Chem.* **1994**, *47*, 979.
(45) Plass, W. *J. Mol. Struct. (THEOCHEM)* **1994**, *315*, 53.
(46) Machado, F. B. C.; Davidson, E. R. *Theor. Chim. Acta* **1995**, *92*, 315.
(47) Stravrev, K. K.; Zerner, M. C. *Chem. Eur. J.* **1996**, *2*, 83.
(48) Dance, I. *ACS Symp. Ser.* **1996**, *653*, 135.
(49) Dance, I. *J. Biol. Inorg. Chem.* **1996**, *1*, 581.
(50) Zhong, S.-J.; Liu C.-W. *Polyhedron* **1997**, *16*, 653.
(51) Dance, I. *Chem. Commun.* **1997**, 165.

investigations focused only on the six-Fe prism located at the center of the FeMo-co. Studies on model systems (such as Fe dimer, trimer) and more realistic structures [$(HC_3S)Fe(\mu^3\text{-}S)_3Fe_3(\mu^2\text{-}S)_3Fe_3(\mu^3\text{-}S)_3Mo$(imidazolyl)(lactic acid derivatives)] support asymmetric, end-on coordination of the nitrogen molecule to one of the tricoordinate four-Fe windows. The concomitant protonation was originated from neighboring bridging sulfurs. A major issue of the previous electronic structure calculations is that they were carried out at nonuniform levels of theory, and the detailed reaction mechanism of the entire N_2 reduction process was never studied.

The aim of this series of studies is to establish a working mechanism for the biological nitrogen fixation by systematic density functional and integrated molecular orbital/molecular mechanical (ONIOM)[55] calculations. In this paper, we present models of the homocitrate and histidine ligands, discuss their importance, as well as the role of the Mo-site of the FeMo-co in the nitrogen fixation process using several mononuclear model systems.

Note that recently experimental kinetic measurements were published studying the role of the homocitrate and histidine ligands using phenylthiolate (PhS^-) reaction of the extracted FeMo-co.[56] The *N*-methylformamide (NMF) extracted wild-type and $NifV^-$ mutant FeMo-cofactors (in which homocitrate is replaced by citrate ligand) bind one molecule of NMF at the tetrahedral Fe center, and NMF $\leftrightarrow$ PhS^- substitution reaction occurs upon addition of PhS^-. The rate of this reaction depends on the other ligands attached to the cluster. If ligands such as CN^-, N_3^-, or H^+ were coordinated to the clusters, no difference between the wild type and mutant FeMo-co was observed. However, when imidazole is bound, the kinetics of the given substitution reaction is different for these clusters. Using a molecular mechanical computational model (MM2), it was shown that (*R*)-homocitrate, but not citrate, is capable of hydrogen bonding to the imidazole ligand on Mo. This interaction perturbs the electron density of the cluster and hence its reactivity.

In the literature, there is only one molecular orbital (MO) study[43] where the extended Hückel method was used for investigating the Mo-site. The N−N bond overlap population (OP) was used as indicator for the N−N bond activation and the net charge on the N atoms as indicator for the proton affinity. It was found that, if N_2 binds to the Mo-site, the N−N bond OP does not change relative to that of the free N_2. The bound (proximal) N has a strong electrophilic character, while the distal N has only a slight nucleophilic character and is not preferred in protonation. Due to the limitation of the method, calculations were performed without geometry optimizations, and they will not be discussed here in more detail.

II. Calculation Procedure and Evaluation of the Models

Quantum chemical calculations of reasonably high level on the real cluster [7Fe-Mo-9S·(homocitrate)] are practically impossible; therefore, one has to construct a workable model system, preserving all essential features of the FeMo-co's Mo-site. Any reasonable model system for studying the Mo-site in the Mo-nitrogenase should include an octahedral Mo atom containing three thiolate ligands, a bidentately coordinated hydroxyl carboxylic acid, and a histidine. (See also Scheme 2, where we present the Mo-site of the FeMo-co in a truncated form with selected distances (Å) taken from the X-ray structure of FeMo-co[5,6,57]).

Scheme 2

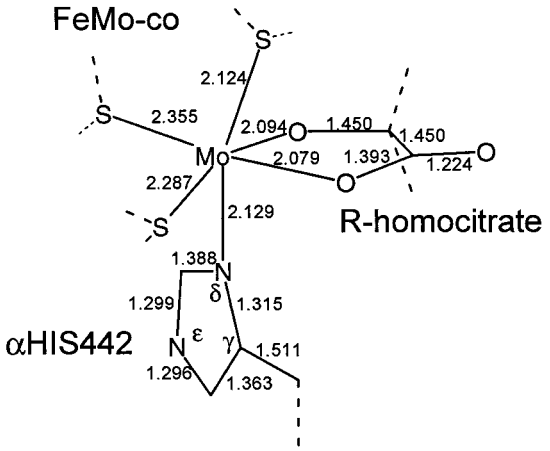

However, due to lack of knowledge about the nature of each individual Mo−ligand bond in the FeMo-co, the proper construction of the ligand environment of Mo atom is not straightforward. First, the thiolate centers of the model presented in Scheme 2 may be simulated (i) either as H_2S, where the S atoms are tricoordinate and the Mo−S bond is a dative Mo←S bond via a lone-pair donation, or (ii) as HS^- ligand which binds to the Mo center via a Mo−S single covalent bond. We have tested both models[58] and have found that only the complex with HS^- ligands led to a well-established coordination sphere of the Mo atom. The replacement of one of the HS^- ligands with the H_2S and geometry optimization led to dissociation of the H_2S ligand, leaving behind a pentacoordinate Mo atom, which is irrelevant as an active site of the FeMo-co. Therefore, below we will simulate S-containing moieties with the HS^- ligands.

The second problem is the simulation of the histidine ligand. Here, we may have also two possibilities: (i) if the uncoordinated N atom (ϵ-N) of the imidazole ring is protonated, then the Mo−N bond is a dative bond and the imidazole ring should be simulated as an imidazolyl ligand, and (ii) if the uncoordinated N atom (ϵ-N) of the imidazole ring is unprotonated, then Mo−N bond has a single bond character and the imidazole ring should be simulated as an imidazolato ligand. Although the short Mo−N distance (2.1 Å) in the FeMo-co suggests the later case, here we studied both possibilities by modeling histidine ligand by the simplified NH_3, NH_2^-, H_2CNH, and H_2CN^- as well as more realistic methylimidazole (MeImH) and methylimidazolate ($MeIm^-$) molecules.

In our studies, the third kind of ligand attached to the Mo-site, homocitrate ligand, was truncated to 2-hydroxypropanoic acid (common name, lactic acid; abbreviated here as lac) by replacing both of the CH_2COOH groups (indicated as dashed lines in Scheme 2) by hydrogens. This substitution leads to inversion in the absolute configuration of the chiral carbon atom (i.e. we used the structure of L(*S*)-lactic acid for modeling the D(*R*)-homocitrate ligand), but since simulations were carried out in an asymmetric-induction-free environment, no effect on structure and stability was attributed to this alteration at the present level of investigation.

(52) Siegbahn, P. E. M.; Westerberg, J.; Svensson, M.; Crabtree, R. H. *J. Phys. Chem. B* **1998**, *102*, 1615.
(53) Dance, I. *Chem. Commun.* **1998**, 523.
(54) Stavrev, K. K.; Zerner, M. C. *Theor. Chem. Acc.* **1997**, *96*, 141.
(55) Dapprich, S.; Komaromi, I.; Byun, K. S.; Morokuma, K.; Frisch, M. J. *J. Mol. Struct. (THEOCHEM)* **1999**, *461*, 1.
(56) Grönberg, K. L.; Gormal, C. A.; Durrant, M. C.; Smith, B. E.; Henderson, R. A. *J. Am. Chem. Soc.* **1998**, *120*, 10613.
(57) Peters, J. M.; Stowell, M. H. B.; Soltis, S. M.; Day, M. W.; Kim, J.; Rees, D. C. *Brookheaven Protein Databank*; code 2MIN.; 1 Apr, 1997.
(58) Szilagyi, R. K.; Musaev, D. G.; Morokuma, K. Unpublished results.

Thus, the model complexes used in this paper are $(HS)_3(NH_3)$-Mo(lac) [**I**], $(HS)_3(NH_2)$Mo(lac) [**II**], $(HS)_3(H_2CNH)$Mo(lac) [**III**], $(HS)_3(H_2CN)$Mo(lac) [**IV**], $(HS)_3$(MeImH)Mo(lac) [**V**], and $(HS)_3$(MeIm)Mo(lac) [**VI**]. Since in this paper we study numerous spin and oxidation states of selected complexes, we adopted the following numbering scheme: $^{2M_S+1}$[**X**]^Z, where **X** refers to a stoichiometry of the model species, $2M_S+1$ is a spin multiplicity (see below for details), and Z is the total charge of the complex. We should note that the most detailed analyses were performed only for the complex [**I**], and only selected examples were studied for other species [**II**]−[**VI**]. To preserve the experimentally reported +4 oxidation state of the Mo atom in the extracted FeMo-co, the total charge associated with the studied systems was set to be −1 for [**I**], [**III**], and [**V**] and −2 for [**II**], [**IV**], and [**VI**]. Also, here we study both the low-spin and the high-spin states for all considered complexes.

Note, below we will also present some preliminary results on the substrate (N_2) coordination to the model [**I**] leading to formation of the complex $(HS)_3(H_3N)Mo(N_2)$(lacH), as well as on the free organic acid ligand and its derivatives.

The geometries of complexes [**I**]−[**VI**], as well as the organic acid ligand and its derivatives were optimized using the B3LYP hybrid density functional theory[59−61] with a standard double-ζ quality basis set (LANL2DZ) associated with the relativistic effective core potential for the molybdenum[62] and the sulfur[63] and valence double-ζ basis set for other atoms.[64] The nature of all obtained equilibrium structures and transition states was tested by performing normal coordinate analyses. All calculations were performed by the Gaussian98 package.[65]

III. Results and Discussion

This section is organized as follows. In subsection 1, we discuss the structure of different protonated forms of the lactic acid. In section 2.A, we analyze geometries of the resting, the one-electron reduced, and the one-electron oxidized forms of the complex [**I**]. In section 2.B, we discuss the single and double protonation of the lactate ligand of complex [**I**]. We compare bidentate and monodentate coordination modes of the homocitrate ligand to the Mo-center and discuss the role of substrate N_2 coordination to the Mo-center in section 2.C. In section 3, we discuss the resting, one-electron reduced, and one-electron oxidized forms of the model complexes [**II**]−[**VI**] with alternative N-ligands along with their protonated forms.

1. The Organic Acid Model Ligands ($lacH_2$, $lacH_c^-$, $lacH_h^-$, lac^{2-}). As seen in Figure 1, where we have presented the calculated energetic and geometric parameters of the L-lactic acid ($lacH_2$) and its different deprotonated forms, $lacH_c^-$, $lacH_h^-$, and lac^{2-}, the $C^{sp^3}-O_h$ bond (1.45 Å) of intact lactic acid molecule ($lacH_2$) is about 0.06 Å longer than the $C^{sp^2}-O_x$ single bond, while the $C^{sp^2}-O_c$ double bond (1.24 Å) is the shortest among all C−O bonds. The calculated values of these C−O bonds are in fair agreement with the data determined by a low-temperature X-ray diffraction technique.[66]

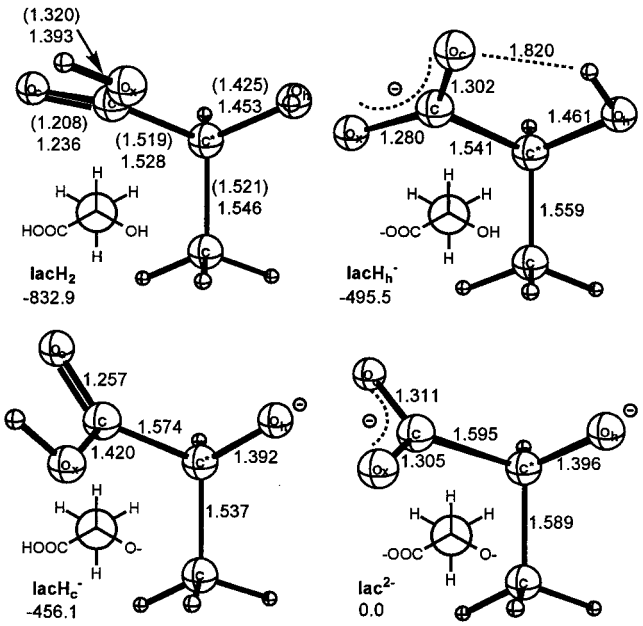

Figure 1. Protonation isomers of the model ligand L-lactic acid [bond lengths in Å and relative energies in kcal mol^{-1}, $E_{total}(lac^{2-})$ = −342.237 524 au]. Solid-state experimental values are given in parentheses.

Deprotonation of the carboxyl group of the lactic acid leads to delocalization of the remained negative charge between the two $C^{sp^2}-O$ bonds. As a result, in ($lacH_h^-$) the two $C^{sp^2}-O$ bond distances become very similar, while the $C^{sp^3}-O_h$ bond distance increased only slightly due to the hydrogen-bonding (H-bonding) interaction with the O_c atom of the carboxylato fragment.

Deprotonation of the hydroxyl group of lactic acid ($lacH_c^-$) decreases the $C^{sp^3}-O_h$ bond distance by 0.06 Å and increases the $C^{sp^2}-O_c$ bond distance by 0.02 Å. In the double deprotonated form of the lactic acid (lac^{2-}), which is the ligand bound to the Mo-center in the unprotonated model complexes [**I**]−[**VI**], the above-mentioned effects are combined; the $C^{sp^2}-O$ bonds become nearly equal and the $C^{sp^3}-O$ is shortened by 0.06 Å compared with those in the unprotonated lactic acid molecule.

As seen in Figure 1, the O_h atom of lac^{2-} has much larger proton affinity than O_x atom, which are calculated to be 495.5 and 456.1 kcal mol^{-1}, respectively. Double protonation of lac^{2-} is calculated to be 832.9 kcal mol^{-1} exothermic process. The protonation energies (ΔE_p) of H_2O and OH^- were calculated to be 181.9 kcal mol^{-1} ($H_2O + H^+ \rightarrow H_3O^+ + \Delta E_p$) and 415.9 kcal mol^{-1} ($OH^- + H^+ \rightarrow H_2O + \Delta E_p$), respectively. Thus, the first protonation of lac^{2-} by H_2O is a spontaneous exothermic process, both at O_h to give $lacH_h^- + OH^-$ (79.6 kcal mol^{-1}) and at O_c to give $lacH_c^- + OH^-$ (40.2 kcal mol^{-1}). The second protonation by H_2O of either $lacH_c^-$ or $lacH_h^-$ to give $lacH_2 + OH^-$ is endothermic (39.1 and 78.5 kcal mol^{-1}, respectively), but it is exothermic (194.9 and 155.5 kcal mol^{-1}, respectively), if their reaction with H_3O^+ is considered to give $lacH_2 + H_2O$.

(59) Becke, A. D. *Phys. Rev. A* **1988**, *38*, 3098.
(60) Lee, C.; Yang, W.; Parr, R. G. *Phys. Rev. B* **1988**, *37*, 785.
(61) Becke, A. D. *J. Chem. Phys.* **1993**, *98*, 5648.
(62) Wadt, W. R.; Hay, P. J. *J. Chem. Phys.* **1985**, *82*, 284.
(63) Hay, P. J.; Wadt, W. R. *J. Chem. Phys.* **1985**, *82*, 270.
(64) Dunning, T. H., Jr.; Hat, P. J. In *Modern Theoretical Chemistry*; Schaefer III, H. F., Ed.; Plenum: New York, 1976; Vol. 3, p 1.
(65) Frisch, M. J.; Trucks, G. W.; Schlegel, H. B.; Scuseria, G. E.; Robb, M. A.; Cheeseman, J. R.; Zakrzewski, V. G.; Montgomery, J. A., Jr.; Stratmann, R. E.; Burant, J. C.; Dapprich, S.; Millam, J. M.; Daniels, A. D.; Kudin, K. N.; Strain, M. C.; Farkas, O.; Tomasi, J.; Barone, V.; Cossi, M.; Cammi, R.; Mennucci, B.; Pomelli, C.; Adamo, C.; Clifford, S.; Ochterski, J.; Petersson, G. A.; Ayala, P. Y.; Cui, Q.; Morokuma, K.; Malick, D. K.; Rabuck, A. D.; Raghavachari, K.; Foresman, J. B.; Cioslowski, J.; Ortiz, J. V.; Stefanov, B. B.; Liu, G.; Liashenko, A.; Piskorz, P.; Komaromi, I.; Gomperts, R.; Martin, R. L.; Fox, D. J.; Keith, T.; Al-Laham, M. A.; Peng, C. Y.; Nanayakkara, A.; Gonzalez, C.; Challacombe, M.; Gill, P. M. W.; Johnson, B. G.; Chen, W.; Wong, M. W.; Andres, J. L.; Head-Gordon, M.; Replogle, E. S.; Pople, J. A. *Gaussian 98, revision A.I*; Gaussian, Inc.: Pittsburgh, PA, 1998.
(66) Schouten, A.; Kanters, J. A.; van Krieken, J. *J. Mol. Struct.* **1994**, *323*, 165.

Table 1. Relative Energies (ΔE in kcal mol^{-1} relative to $E_{total}(^3[\mathbf{I}]^-) = -408.804\,060$ au), the Expectation Value of S^2, Mulliken Atomic Gross Spin Densities (ρ_s), Atomic charge (q), and Atomic Orbital Gross Populations of Various O$_x$idation and Spin States of Model Complex [**I**]

state of the Mo-site (Z)	Mo oxidation state	spin $2M_S+1$	symbol	ΔE	$\langle S^2\rangle$	ρ_s(Mo)	Mo atomic orbital gross population 5s	5p	4d	q(Mo)
oxidized	V	2	^{2}[**I**]	68.47	0.76	1.01	0.41	0.69	4.54	+0.36
(0)	(d^1)	4	^{4}[**I**]	88.54	3.77	1.89	0.37	0.59	4.63	+0.36
resting	IV	1	^{1}[**I**]	9.20	0.00	0.00	0.38	0.69	4.56	+0.33
(−1)	(d^2)	3	^{3}[**I**]	0.00	2.02	1.98	0.38	0.67	4.55	+0.38
		5	^{5}[**I**]	26.5	6.01	2.71	0.32	0.60	4.68	+0.39
reduced	III	2	^{2}[**I**]^2	48.28	1.61	1.04	0.35	0.72	4.56	+0.29
(−2)	(d^3)	4	^{4}[**I**]^2	34.65	3.76	2.91	0.35	0.71	4.50	+0.33
		6	^{6}[**I**]^2	116.8	8.76	3.71	0.35	1.29	4.56	0.56

2. Modeling Mo−Homocitrate Interaction. In this section, the effects of the one-electron reduction and oxidation, single and double protonation, and substrate coordination to the structure and stability of the complex [**I**] were discussed in detail. We do this with the intention to provide basic foundations for the further studies of the larger cluster models of the Mo-site. In addition, since we do not have experiment results, we discussed these data in a systematic way in sections A and B.

A. Structure and Stability of [I]^Z, [(HS)$_3$(H$_3$N)Mo(lac)]^Z. The optimized structures of the ground and first excited states of this complex in its oxidized ($Z = 0$), resting ($Z = -1$), and reduced ($Z = -2$) forms are shown in Figure 2. Their relative energies and selected electronic properties are given in Table 1.

Resting Form of the Complex [I]$^-$. As shown in Table 1, the ground state of the resting form of complex [**I**] ($Z = -1$) is the triplet with two unpaired electrons located on the Mo center (ρ_s(Mo) = 1.98e). The oxidation state of Mo in this complex is IV (for more details see below), which is consistent with experimental observations. The singlet state (^{1}[**I**]$^-$) with two electrons located in the same Mo d-orbital and paired lies about 9 kcal mol^{-1} above the ground state ^{3}[**I**]$^-$. The quintet state with four unpaired electrons is calculated to be energetically much higher (27 kcal mol^{-1}); this state requires an electron excited from the metal−ligand bonding orbital and, as expected, shows spin densities on the S atoms (+1.29e).

The results presented in Figures 1 and 2 show that the coordination of the lactate ligand (lac^{2-}) to the (HS)$_3$Mo(NH$_3$) fragment increases the C$^{sp^3}$−O$_h$ bond distance by 0.05 Å, close to the value calculated for the lactic acid (lacH$_2$). The C$^{sp^2}$−O$_x$ distance does not change significantly and increases only by 0.03 Å, while the C$^{sp^2}$−O$_c$ bond restores its double bond character. We consider the calculated Mo−O$_h$ and Mo−O$_x$ bond distances (1.97 Å and 2.10 Å, respectively) as references for the nonactivated Mo−O bonds in the resting state of complex [**I**]. Comparison of the calculated Mo−O distances with the available X-ray results (see Scheme 2) shows that the calculated Mo−O$_h$ and Mo−O$_x$ bond distances are about 0.12 and 0.02 Å shorter than the relevant experimental data, respectively.

One-Electron Reduced Form of Complex [I]$^{2-}$. As expected, the ground state of the complex [**I**]$^{2-}$ has a quartet spin state ($\langle S^2\rangle = 3.76$) with 2.91e spin density on the Mo atom. Thus, the Mo ion in ^{4}[**I**]$^{2-}$ formally has an oxidation state of III. The spin density value clearly shows that the additional electron is located on one of the d-orbitals of the Mo atom. The doublet state lies about 14 kcal mol^{-1} higher. As seen in Figure 2, one-electron reduction of the complex ^{3}[**I**]$^-$ significantly changed the geometries of the lactate fragment. For example, the Mo−O$_h$ and Mo−O$_x$ bonds are elongated by 0.10 and 0.04 Å, respectively.

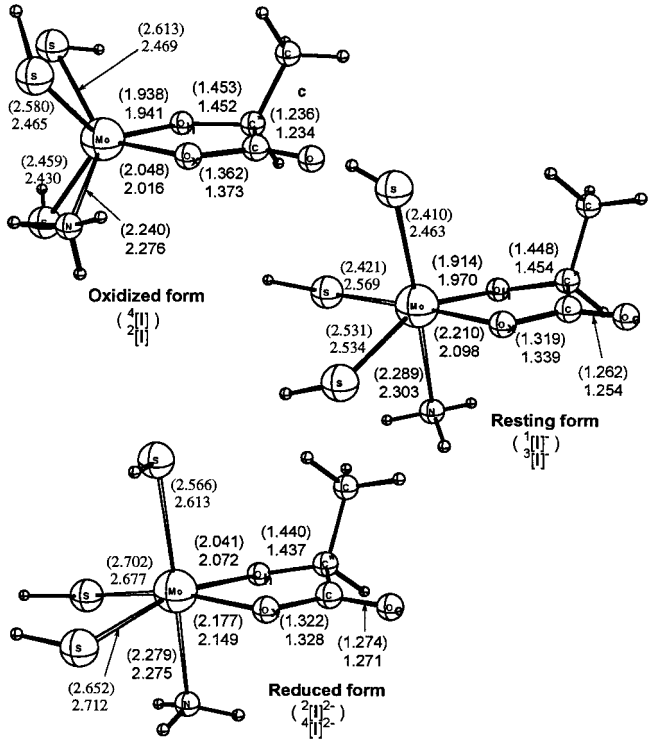

Figure 2. Molecular structure of resting, reduced, and oxidized forms of the model complex [**I**] (bond lengths in Å).

The one-electron reduction of the complex ^{3}[**I**]$^-$ is not favorable energetically; the complex ^{3}[**I**]$^-$ has a negative electron affinity of 35 kcal mol^{-1}.

One-Electron Oxidized Form of the Complex [I]^0. The one-electron oxidized form of the complex [**I**] was also studied for the sake of completeness, and the ground state was found to be a doublet state, ^{2}[**I**], with one unpaired electron located on the Mo d-manifold. By oxidation of ^{3}[**I**]$^-$, one of the Mo d-electrons was removed and the oxidation number of Mo was changed from IV to V. As seen in Figure 2, the oxidation of ^{3}[**I**]$^-$ to ^{2}[**I**] does not cause large changes in the Mo−O$_h$ and C$^{sp^3}$−O$_h$ bond distances, while it reduces the Mo−O$_x$ bond distance by 0.08 Å and increases the C$^{sp^2}$−O$_x$ bond by 0.03 Å. The coordination geometry (mainly the angles) around the Mo is also significantly altered.

B. Protonation of Organic Ligand of Complexes [I], [IH]$^{Z+}$, where $Z = +1, 0, -1$. The optimized structures of the complexes [**IH$_c$**]$^{Z+}$, [**IH$_x$**]$^{Z+}$, and [**IH$_h$**]$^{Z+}$ corresponding to the single protonation of the organic ligand at its O$_c$, O$_x$, and O$_h$ atoms, respectively, are shown in Figure 3. Their relative energies are summarized in Table 2. As seen from comparison of the relevant geometrical parameters for unprotonated (Figure 2) and protonated (Figure 3) forms of the complex [**I**], as well

Table 2. Energy of Protonated States (ΔE_p) Relative to the Relevant Unprotonated Forms, Energy of One-Rtep (coupled) Reduced + Protonated States (ΔE_{rp}) Relative to the Resting State (^{3}[**I**]$^-$) of Model Complexes [**I**] in Various Oxidation and Spin States

		ΔE_p, kcal mol^{-1} $^{2M_S+1}$[**I**]^Z + H$^+$ → $^{2M_S+1}$[**IH**]$^{Z+1}$ + ΔE_p $^{2M_S+1}$[**I**]^Z + 2H$^+$ → $^{2M_S+1}$[**IHH**]$^{Z+2}$ + ΔE_p					ΔE_{rp}, kcal mol^{-1} ^{3}[**I**]$^-$ + H$^+$ + e$^-$ → $^{2M_S+1}$[**IH**] + ΔE_{rp}		
state (Z)	$2M_S$+1	[**IHc**]$^{Z+1}$	[**IHx**]$^{Z+1}$	[**IHh**]$^{Z+1}$	[**IHhHx**]$^{Z+2}$	[**IHhHc**]$^{Z+2}$	[**IHc**]$^{Z+1}$	[**IHx**]$^{Z+1}$	[**IHh**]$^{Z+1}$
oxidized (0)	2	218.5	214.0	212.2					
resting (1)	1	313.7	315.7	315.7					
	3	306.8	307.3	311.4					
reduced (2)	2	390.5	396.6	405.3			342.3	348.4	357.1
	4	386.3	389.5	404.2	706.5	707.8	351.6	354.8	369.5

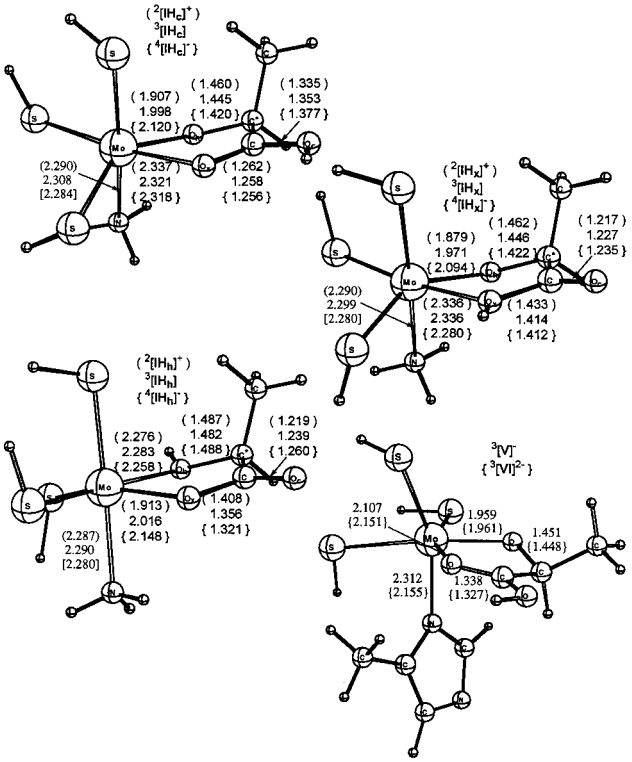

Figure 3. Optimized structures (bond lengths in Å) of complexes [**IH**]$^{Z+}$, ^{3}[**V**]$^-$, and ^{3}[**VI**]$^{2-}$, where $Z = +1, 0, -1$.

as its derivatives, the protonation of any oxygen atom of the organic ligand causes remarkable geometrical changes, in particular, in the Mo−O bond lengths. For example, protonation of the complex ^{3}[**I**]$^-$ on O_c or O_x atom elongates the Mo−O_x bond by 0.24 Å, while it does not change significantly the Mo−O_h bond distance. In contrast, protonation on the O_h atom increases the Mo−O_h bond distance by 0.31 Å, and reduces the Mo−O_x bond distance only by 0.08 Å.

Among the three protonation sites of the lactate ligand, the protonation of the O_c atom causes the most significant changes. The O_c atom becomes a bivalent sp^3 hybrid with elongated C−O_c bond length, while the C−O_x bond length is shortened, indicating the double bond character, which also results in elongation of the Mo−O_x bond. If the O_x atom is protonated, the Mo−O_x single bond is again transformed to a weaker interaction through one of the lone pair of the O_x atom. In this case the C−O_c bond does not change much. Note that in the two cases presented above, the nature of the Mo−O_x bonds is not the same. In the first case (protonation on O_c atom) the Mo−O_x can be considered as a Mo−O^{sp^2} lone pair interaction, while in the second case it has Mo−O^{sp^3} lone pair character. The Mo−O_h bond on the other side of the complex virtually remains unaltered upon protonation of the carboxylic group. If

Table 3. Mo−Ligand Binding Energies of the N- and O-Containing Ligands in the Selected Complexes

complex	ligand (L)	ΔE, kcal mol^{-1}
^{3}[**I**]$^-$	NH_3	12.1
^{3}[**II**]$^{2-}$	NH_2^-	33.2
^{3}[**III**]$^-$	MeImH	6.3
^{3}[**IV**]$^{2-}$	MeIm$^-$	24.8
^{3}[**I**]$^-$	lac^{2-}	346.9
^{3}[**IH$_h$**]	lacH$_h^-$	162.8
^{3}[**IH$_x$**]	lacH$_c^-$	198.0
^{3}[**IH$_c$**]	lacH$_c^-$	197.6
^{4}[**I**]$^{2-}$	lac^{2-}	151.2
^{4}[**IH$_h$**]$^-$	lacH$_h^-$	59.8
^{4}[**IH$_x$**]$^-$	lacH$_c^-$	84.6
^{4}[**IH$_c$**]$^-$	lacH$_c^-$	81.4
^{4}[**IH$_h$H$_x$**]	lacH$_2$	24.8
^{4}[**IH$_h$H$_c$**]	lacH$_2$	26.1
^{3}[**IH$_x$**]·(N_2)	N_2	4.8
^{4}[**IH$_x$**]$^-$·(N_2)	N_2	6.7

Table 4. A Representative Set of Bond Distances[a] (in Å) and Relative Energies (in kcal mol^{-1}) of the Complexes [**I**]−[**IV**] and Their Protonated Forms

complex	relative energies	Mo−N (L)	Mo−O_x	Mo−O_h	C−O_x	C−O_h	C−O_c
			N-ligand = NH_3				
^{3}[**I**]$^-$	0.0	2.303	2.098	1.970	1.339	1.454	1.254
^{3}[**IH$_c$**]	306.8	2.308	2.321	1.998	1.258	1.445	1.353
^{3}[**IH$_x$**]	307.3	2.299	2.336	1.971	1.414	1.446	1.227
^{3}[**IH$_h$**]	311.4	2.290	2.016	2.283	1.357	1.482	1.239
			N-ligand = NH_2^-				
^{3}[**II**]$^{2-}$	0.0	1.966	2.156	1.989	1.324	1.443	1.270
^{3}[**IH$_c$**]$^-$	−382.0	1.963	2.349	2.025	1.252	1.425	1.375
^{3}[**IH$_x$**]$^-$	−386.8	1.967	2.259	1.998	1.403	1.432	1.234
^{3}[**IH$_h$**]$^-$	−395.5	1.966	2.054	2.280	1.334	1.479	1.252
			N-ligand = (H)NCH_2				
^{3}[**III**]$^-$	–	2.261	2.098	1.971	1.338	1.453	1.254
			N-ligand = NCH_2^-				
^{3}[**IV**]$^{2-}$	–	1.921	2.149	1.996	1.325	1.441	1.269
			N-ligand = HMeIm				
^{3}[**V**]$^-$	–	2.312	2.107	1.959	1.338	1.451	1.256
			N-ligand = MeIm$^-$				
^{3}[**VI**]$^{2-}$	–	2.155	2.151	1.961	1.327	1.448	1.265
			Experiment [see ref 1]				

[a] The details of calculated geometric parameters of these complexes are presented in the Supporting Information.

the O_h atom is protonated, the Mo−O_h bond becomes activated and, in addition, the Mo−O_x bond shortens. In the resting form, the calculated protonation energies are close to each other and decrease via O_h (311.4 kcal mol^{-1}) > O_x (307.3 kcal mol^{-1}) ≈ O_c (306.8 kcal mol^{-1}) (Table 4).

The reduced form, [**IH$_c$**]$^-$, shows similar tendencies as the resting form in bond lengths and protonation energies. The longest Mo−O bond again is found to be the Mo−O_x, 2.318

Å, in the complex $^4[\mathbf{IH_c}]^-$, while the largest change (relative to the unprotonated values) occurs on the Mo−O_h bond in the complex $^4[\mathbf{IH_h}]^-$ (Δ = 0.19 Å). The calculated protonation energies changes in the order O_h (404.2 kcal mol^{-1}) > O_x (389.5 kcal mol^{-1}) > O_c (386.3 kcal mol^{-1}), and the O_h atom is again the most favorable site for protonation.

An additional outcome of this systematic investigation is the comparison of the one-electron reduction, single protonation, and the coupled protonation/reduction process of the resting state complex. The one-electron reduction $^3[\mathbf{I}]^- + e^- \rightarrow {}^4[\mathbf{I}]^{2-}$ (ground state to ground state) is calculated to be 35 kcal mol^{-1} endothermic (Table 1). The single protonation $^3[\mathbf{I}]^- + H_2O \rightarrow {}^3[\mathbf{IH}] + OH^-$ is also found to be endothermic by 104 kcal mol^{-1} (on O_h) and 109 kcal mol^{-1} (on O_c or O_x) (Table 2). The coupled protonation/reduction process $^3[\mathbf{I}]^- + H_2O + e^- \rightarrow {}^4[\mathbf{IH}]^- + OH^-$ is still endothermic by 46 kcal mol^{-1} (at O_h), 64 kcal mol^{-1} (at O_c), and 61 (at O_x) kcal mol^{-1}. Meantime, the one-electron reduction of the protonated resting states $^3[\mathbf{IH}] + e^- \rightarrow {}^4[\mathbf{IH}]^-$ is an exothermic process by 58 kcal mol^{-1} (for $^3[\mathbf{IH_h}]$), 45 kcal mol^{-1} (for $^3[\mathbf{IH_c}]$), and 48 kcal mol^{-1} (for $^3[\mathbf{IH_x}]$), but the protonation of the reduced form $^4[\mathbf{I}]^{2-} + H_2O \rightarrow {}^4[\mathbf{IH}]^- + OH^-$ is again endothermic by 12 kcal mol^{-1} (via O_h), 30 kcal mol^{-1} (via O_c), and 26 kcal mol^{-1} (via O_x). The protonation can be exothermic if a stronger acid than H_2O (e.g. H_3O^+) is considered.

Thus, the protonation energies of the resting and reduced forms of [**I**] decrease via O_h > O_x ≈ O_c. However, in the oxidized form of [**I**], this trend is the opposite. Also, as expected, the protonation energy (ΔE_p, see Table 2) decreases in the order, reduced form > resting form > oxidized form.

It is worth mentioning the effect of protonation on the energy differences between the ground and excited states. As can be seen in Table 2, the singlet−triplet and doublet−quartet energy gaps of the resting and one-electron reduced forms of [**I**] decrease upon protonation, from 9.2 to 4.3 kcal mol^{-1} and from 13.6 to 1.1 kcal mol^{-1}, respectively.

In Table 3 we have presented various calculated Mo−ligand binding energies. As seen from this table, Mo−organic ligand interaction energy decreases dramatically upon protonation and reduction. In the resting form of the complex [**I**] ($^3[\mathbf{I}]^-$), the lactate ligand is tightly bound to the Mo atom (BDE = 347 kcal mol^{-1}). Upon protonation, the Mo−lactate binding energy reduces by 40−55%, depending on the site of protonation. If the O_h atom is protonated, the organic acid ligand binds covalently through the O_x atom and the HO_h group is only weakly coordinated. Therefore, the binding energy is smaller (163 kcal mol^{-1}) than if the O_x or O_c is protonated (198 kcal mol^{-1}), where the stronger Mo−O_h bond remains unaltered or even strengthened, as seen by the decrease of the Mo−O_h distance. The difference between the experimental and calculated Mo−O_h distance can be rationalized by assuming that the O_h proton is interacting with a neighboring water molecule/amino acid residue in the experiment, while in the calculated model it is naked.[67]

In case of the one-electron reduced form ($^4[\mathbf{I}]^{2-}$), the Mo−lactate binding energy of the unprotonated lactate ligand is calculated to be about 151 kcal mol^{-1}, which reduces by an additional 35−70% upon the first protonation. Note that our results indicate that a stronger activation by protonation (or larger protonation energy) corresponds to a weaker Mo−lactate interaction, for both complexes $^3[\mathbf{I}]^-$ and $^4[\mathbf{I}]^{2-}$. Indeed, for both cases, the protonation of lactate ligand via O_h atom is energetically more favorable than those of O_c and O_x atoms, while the Mo−lacH_h^- interaction is calculated to be weaker than Mo−lacH_x^- and Mo−lacH_c^-.

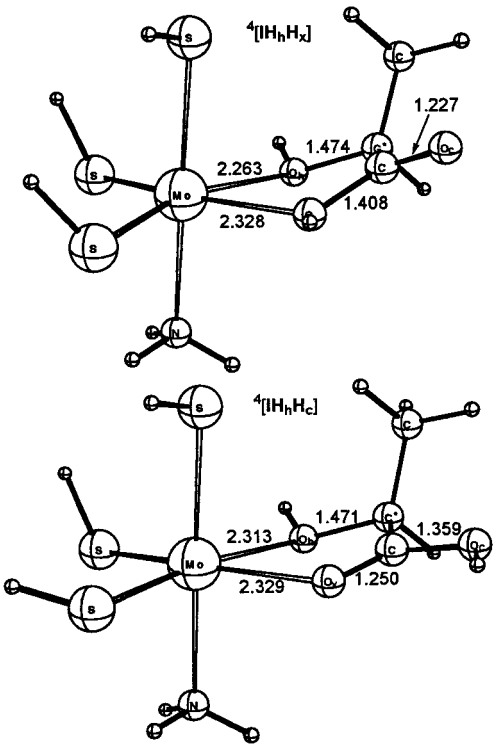

Figure 4. Optimized structure (bond lengths in Å) of the one-electron reduced, double-protonated forms of the complex [**I**].

C. Bi- vs Monodentate Coordination and Substrate Coordination. The results presented above indicate that, while the single protonation of the complex [**I**] and its derivatives on various O atoms increases the asymmetricity in the Mo−O bonds and reduces the Mo−lac binding energies, it does not change the coordination mode of the organic ligand to the Mo-center. In other words, the protonation of the complex [**I**] and its derivatives on various O atoms of the organic ligand keeps the organic ligand bidentate-coordinated to the Mo-center and does not reduce the coordination number of the Mo-center spontaneously. If the Mo-center stays hexacoordinate, then it cannot directly bind the substrate and cannot take part in the N_2 fixation and reduction process. Therefore, we believe that decrease of coordination number of the Mo-center of FeMo-co from six to five is one of the important questions from the mechanistic point of view, and we decided to study it in more detail.

Since the double protonation of the lactate ligand dramatically reduces the Mo−lactate binding energy in $^4[\mathbf{I}]^{2-}$ (from 151 kcal mol^{-1} to about 25 kcal mol^{-1}, as seen in Table 3), one may expect the double protonation of organic ligand to be one of the factors facilitating the bidentate ↔ monodentate rearrangement in the FeMo-co. The calculated energies and structures of the one-electron-reduced, double-protonated forms of the complex $^3[\mathbf{I}]^-$ are presented in Table 2 and Figure 4, respectively. As seen in Figure 4, despite the lengthening of the Mo−O bonds upon double protonation of lactate ligand, the Mo-center in $^4[\mathbf{IHH}]$ does not change its a six-coordinated environment, while a remarkable puckering of 20−30° of the Mo−lactate ring is found. In the nonprotonated and single-protonated forms of $^4[\mathbf{I}]^{2-}$ this ring was nearly flat.

To reveal the kinetic and thermodynamic stability of the Mo-complex with monodentate lactate ligand, at first, we tried to

(67) Szilagyi, R. K.; Musaev, D. G.; Morokuma, K. *J. Mol. Struct. (THEOCHEM),* **2000**, *506*, 131.

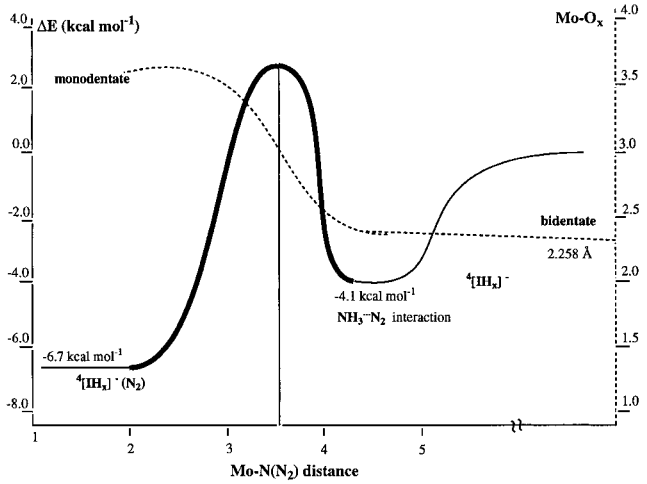

Figure 5. Relaxed potential energy scan for N_2 coordination to the complex $^4[\mathbf{IH_x}]^-$ (solid line relative energy and dashed line $M-O_x$ distance).

locate a structure corresponding to the single-protonated complexes $^3[\mathbf{IH_x}]$ and $^3[\mathbf{IH_h}]$ as two of the most stable protonated isomers of the resting form. Any attempt to locate monodentate complex as a stationary point failed, and the geometry optimization from a monodentate structure always converged to a bidentate structure. These results indicate that single-protonated complexes $^3[\mathbf{IH_x}]$ and $^3[\mathbf{IH_h}]$ have no structures corresponding to the monodentate coordination of lactate (homocitrate) ligand. Second, we have performed a partial geometry optimization to simulate the dissociation of one of the legs of the bidentate lactate ligand. These calculations demonstrated that the potential energy surface of the bidentate ↔ monodentate rearrangement is flat with only one minimum corresponding to the bidentate coordination of lactate ligand: the energy difference between equilibrium bidentate and an assumed monodentate structures (with the $Mo-O_x$ distance frozen at ~4.3 Å) is about 8.8 kcal mol^{-1}. Therefore, one may expect that the coordination of the substrates or solvent molecules at the Mo-center can facilitate opening one of the "legs" of the homocitrate (in our case, lactate) ligand. Here, as a substrate, we considered a N_2 molecule because of its relevance to the nitrogen fixation process, and as a model for the Mo-site of FeMo-co, we chose the resting ($^3[\mathbf{IH_x}]$) and one-electron reduced ($^4[\mathbf{IH_x}]-$), single-protonated forms of the complex $^3[\mathbf{I}]^-$. Since the calculation of the transition state associated with simultaneous substrate coordination and lactate "leg" opening is too complicated, we scanned the potential energy surface by optimizing geometries at various fixed values of the $Mo-N_2$ distance. The $Mo-N_2$ interaction energy and $Mo-O_x$ as functions of the $Mo-N_2$ distance are presented in Figure 5.

At large Mo−N distances the N_2 molecule can interact with other ligands. For example, at 5 Å the N_2 interacts with NH_3 ligand, which leads to about 4.0 kcal mol^{-1} stabilization energy due to a $H_2NH\cdots N_2$ interaction. The organic acid remains bidentate at this point. When the N_2 is approaching the Mo center, at about 4 Å, the lactate ligand starts to open one of its "legs". The transition state (TS) of this process is located at around Mo−N = 3.5 Å. The energetic barrier corresponding to this TS is calculated to be about 7 kcal mol^{-1}, which can be considered as an upper limit of the real barrier. This barrier is even smaller if the barrier is calculated from the dissociation limit $N_2 + {}^4[\mathbf{IH_x}]^-$ (~3 kcal mol^{-1}). Any attempt to locate the real TS failed, and calculations converged to the structure

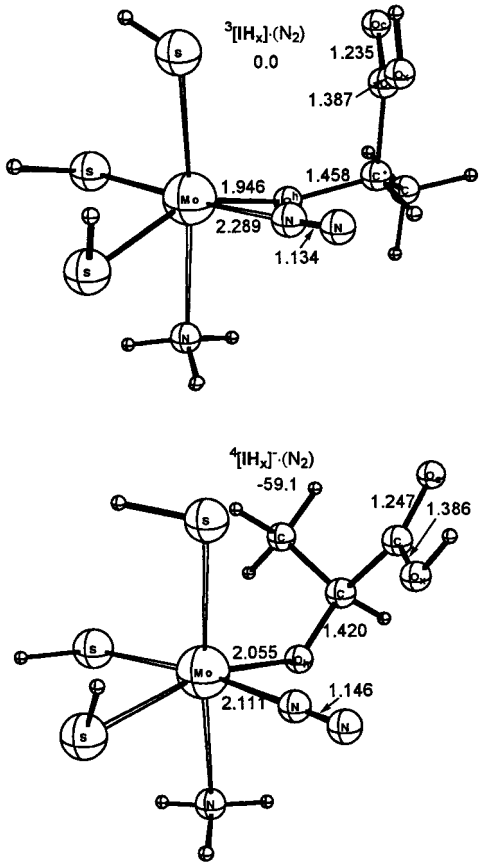

Figure 6. Structure and relative energies of complexes $^3[\mathbf{IH_x}]\cdot(N_2)$ and $^4[\mathbf{IH_x}]^-\cdot(N_2)$ (bond lengths in Å and relative energies in kcal mol^{-1}).

containing the monodentate coordinated organic ligand and coordinated N_2 molecule as shown in Figure 6.

As seen in Figure 6, where we have presented the optimized structures of the complexes $^3[\mathbf{IH_x}]\cdot(N_2)$ and $^4[\mathbf{IH_x}]^-\cdot(N_2)$, one of the Mo−O bonds (namely $Mo-O_x$) is broken, and the lactate ligand is very much twisted around the remaining $Mo-O_h$ and $C-O_h$ bonds, while the uncoordinated carboxyl group remains as close as possible to the Mo center (average $Mo-O_x$ distance is about 3.7 Å).

The interaction of N_2 with the metal is stronger in the one-electron reduced form $^4[\mathbf{IH_x}]^-\cdot(N_2)$ than in the resting form $^3[\mathbf{IH_x}]\cdot(N_2)$. The N−N distance is stretched by 0.013 Å in the former but only by 0.001 Å in the latter, relative to the free N_2 distance of 1.133 Å at this level of theory. Similarly, the Mo−N distance is shorter (2.111 Å) in the former than in the latter (2.289 Å). As a result, the N_2 binding energy relative to the bidentate complex $^4[\mathbf{IH_x}]^-$ is calculated to be stronger (6.7 kcal mol^{-1}) in the former than in the latter (4.8 kcal mol^{-1}).

The results presented above indicate that neither single/double protonation nor reduction of the model complex can reduce the coordination number of the Mo-center spontanously. It happens only upon substrate (N_2) coordinating to the Mo-center of the single-protonated forms of the complex [**I**]. *Thus, one electron reduction, single-protonation, and substrate coordination facilitate the bidentate ↔ monodentate rearrangement of the homocitrate (lactate) ligand of FeMo-co.*

3. Modeling the Mo−*Histidine* Interaction of the FeMo-co. Now, we will study the nature of the Mo−N bond, which is an another issue not clearly addressed in the literature upon modeling of the nitrogenase. The above presented results for the complex [**I**] show that the NH_3 is not a good model for

histidine; the calculated Mo−N distance is much longer (about 0.2 Å) than the experimentally reported value for the real complex. Therefore, we also examine the possibility of modeling of *His* by NH_2^- ligand, by calculating the structures of the complex $[(HS)_3(H_2N)Mo(lac)]^{2-}$, $[\mathbf{II}]^{2-}$. The important bond distances of complex $[\mathbf{II}]^{2-}$ and its various protonated derivatives, $[\mathbf{IIH_c}]^-$, $[\mathbf{IIH_x}]^-$, and $[\mathbf{IIH_h}]^-$, calculated at their ground triplet states are given in Table 4. The complete geometrical parameters of these complexes are given in the Supporting Information.

As expected, the substitution of NH_3 ligand in [I] with NH_2^- significantly reduces the Mo−N bond length. In the resting form of the resulted complex $^3[\mathbf{II}]^{2-}$, the calculated Mo−N bond length is about 0.3 and 0.2 Å shorter than that in the complex $^3[\mathbf{I}]^-$ and the experimental value, respectively. These data indicate that the NH_2^- is also not a proper model of the histidine ligand, too.

It is worthwhile to mention that, formally, complex [**II**] can be also considered as the N-deprotonated form of complex [**I**]. This deprotonation increases the electron density on the Mo-atom and more specifically in the Mo−N bond region, which is clearly indicated, for example, by the elongation of Mo−O distances in $^3[\mathbf{II}]^{2-}$, relative to $^3[\mathbf{I}]^-$. One should note that, upon protonation of the lactate ligand of the complex $^3[\mathbf{II}]^{2-}$, the Mo−N bond virtually remains unchanged; as was found for the complex $^3[\mathbf{I}]^-$, the Mo−O and C−O distances become slightly longer and shorter than in the relevant complex [**I**], respectively. This suggests that the nature of the Mo−N bond itself has an insignificant effect on the bidentate ↔ monodentate rearrangement of the lactate ligand.

Thus, neither NH_3 nor NH_2^- is a proper ligand for describing the Mo−*His* interaction in the Mo-site of the nitrogenase, which can be explained on the basis of the following discussions. Both of these N-ligands have an sp^3 N atom, which is rather different from the quasi-sp^2 N atoms of the imidazole ring. Formally, within the imidazolyl type of coordination of the histidine residue, the Mo−N bond is formed by the lone pair of the sp^3 N, while the another N atom of the ring is protonated and its lone-pair is involved in the π-electron conjugation. The NH_3 ligand as a model of imidazolyl has the available lone-pair for Mo−N bond formation, but it has no contribution from the π-electron conjugation. On the other hand, within the imidazolato type of coordination of the histidine residue, the Mo−N bond has covalent bond character involving the lone pair of the N atom and the π-electron conjugation. The uncoordinated N atom of the ring now has pure sp^3 character and has an available lone pair for interaction. The NH_2^- ligand intended to model this situation can only form a covalent bond with the Mo, but its lone pair cannot be involved in conjugation. On basis of these discussions, the use of the methylimine ($HNCH_2$) could be a more reasonable alternative to modeling of the imidazole ligand. Therefore, we have optimized the structures of ground states of complexes $[(HS)_3(H_2CNH)Mo(lac)]^-$, $[\mathbf{III}]^-$, and $[(HS)_3(H_2CN)Mo(lac)]^{2-}$, $[\mathbf{IV}]^{2-}$, with $(H)N{=}CH_2$ and $(N{=}CH_2)^-$ as a model of the *His* residue, respectively. A representative set of their calculated important bond lengths are also given in Table 4.

The tendency of Mo−N bond distance for complexes [**I**] and [**II**] obtained above and shown in Table 4 was also observed for complexes $[\mathbf{III}]^-$ and $[\mathbf{IV}]^{2-}$. The $HN{=}CH_2$ coordinates to Mo via a weak dative bond and gives longer bond length (0.13 Å) than the experimental value of the Mo−N bond. While the $(N{=}CH_2)^-$ ligand gives a strong Mo−N bond about 0.21 Å shorter than the experimental distance. These data indicate that the methylimine derivatives are also not a proper model for describing the Mo−*His* interaction in FeMo-co.

Therefore, we performed additional analyses with more realistic N-ligands, MeImH and $MeIm^-$, i.e., complexes $[(HS)_3(MeImH)Mo(lac)]^-$, $[\mathbf{V}]^-$, and $[(HS)_3(MeIm)Mo(lac)]^{2-}$, $[\mathbf{VI}]^{2-}$, respectively. Molecular structures of the complexes $^3[\mathbf{V}]^-$ and $^3[\mathbf{VI}]^{2-}$ and some of their protonated forms are given as Supporting Information. Here, we will only discuss the important bond distances of the complexes $^3[\mathbf{V}]^-$ and $^3[\mathbf{VI}]^{2-}$, given in Table 4. As seen in Table 4, in the complex $^3[\mathbf{V}]^-$ the Mo−N bond distance (2.312 Å) is again longer than its experimental value (2.129 Å). However, in the complex $^3[\mathbf{VI}]^{2-}$ it is 2.155 Å, which is in excellent agreement with experiment. On the basis of this comparison, we could conclude that (1) $MeIm^-$ is the smallest acceptable model of the *His* residue properly describing of the Mo−*His* interaction in the FeMo-co and (2) the *His* residue is attached to the FeMo-co through a single, covalent Mo−N bond.

Note, in the X-ray structures, the β-N relative to the methyl substituent of the imidazole ring (δ-N in the histidine residue) is bound to the Mo-center in the resting state of the nitrogenase enzyme. All previous experimental and theoretical studies assumed that the noncoordinated nitrogen of the imidazole ring (ϵ-N in the histidine residue) is protonated. However, our aforementioned results clearly indicate that the ϵ-N of the FeMo-co bound histidine residue is NOT protonated. As a consequence, the cluster is very tightly bound to the protein matrix via a strong covalent bond between the molybdenum and the δ-N of the histidine residue. The proton from the free histidine residue might be located around the FeMo-co. One of the best candidates that could intercept this proton is the hydroxyl oxygen of the homocitrate ligand. This assumption is also supported by additional studies of the first solvation shell of the HC ligand (see part II[67]).

An obvious question is how the histidine residue prevents its protonation in a system where proton sources are located nearby (a water pool exists around the homocitrate ligand in the real system, as is seen in the X-ray structure). Here comes the role of the homocitrate ligand. The longer carboxylic arm of the homocitrate is long enough to prevent the protonation of the ϵ-nitrogen. The carboxylic group is located about 4 Å above the imidazole ring in a nearly parallel position (plane-to-plane deviation is less than 2°), as it is seen in the X-ray structure of the FeMo-co (Scheme 1). One may consider the longer carboxyl arm of the HC ligand as a shield above the imidazole ring protecting against protonation. If a citrate (2-hydroxy-propane-1,2,3-tricarboxlic acid) is used as the organic acid ligand in mutated strains, then the shorter carboxylic arms are not capable of preventing the protonation. In this case, the FeMo-co will be only loosely bound to the matrix, destroying the finely tuned position within the catalytic peptide cavity, which can lead to loss in catalytic activity.

IV. Conclusions

From results and discussion presented above, we can draw the following conclusions.

The studies on the resting and reduced forms of the complex [**I**] show that the protonation of the homocitrate ligand (lactate ligand in our case) via its hydroxyl oxygen, O_h, is more favorable than via carboxylic oxygen atoms, O_c or O_x. However, in oxidized form of [**I**], this trend is the opposite. In general, the protonation of the homocitrate ligand elongates the Mo−protonated oxygen distance by 0.2−0.3 Å compared with its nonprotonated forms and reduces the Mo−lactate binding energy, while only slightly changes the Mo−N bond.

The spontaneous bidentate ↔ monodentate rearrangement of the homocitrate (lactate) ligand, which is proposed to be crucial for the catalytic activity of the Mo-center of FeMo-co, does not occur either upon single and even double protonation or one-electron reduction or oxidation. However, it can happen only upon substrate coordination to the Mo-center of the single-protonated forms of the complex [**I**]. Thus, at least one electron (to reduce a system), one proton (to protonate the carboxylic leg), and a substrate molecule are needed for the bidentate ↔ monodentate rearrangement of the homocitrate (lactate) ligand of FeMo-co.

The smallest acceptable model of *His* ligand in FeMo-co is found to be methylimidazolate ($MeIm^-$) rather than NH_3/NH_2^- or the H_2CNH/H_2CN^-. Our studies suggest that the ϵ-N of the FeMo-co-bound *His* residue is not protonated and the cluster is tightly bound to the protein matrix via a strong $Mo-N^{\delta}$ bond. We also suggest that the longer carboxylic arm of the homocitrate is preventing the protonation of the ϵ-nitrogen.

Acknowledgment. The present research is in part supported by a grant (CHE-9627775) from the National Science Foundation. Acknowledgment is also made for generous support of computing time at Emerson Center of Emory University, US National Center for Supercomputing Applications (NCSA), and Maui High Performance Computer Center (MHPCC).

Supporting Information Available: Details of calculated geometric parameters and molecular structures of these complexes and some of their protonated forms are given. This material is available free of charge via the Internet at http://pubs.acs.org.

IC000188N